Journal of Zhejiang University-SCIENCE A (Applied Physics & Engineering)
ISSN 1673-565X (Print); ISSN 1862-1775 (Online)
www.zju.edu.cn/jzus; www.springerlink.com
E-mail: jzus@zju.edu.cn

An energy harvester combining a piezoelectric cantilever and a single degree of freedom elastic system*

Hong-yan WANG†[1,2], Xiao-biao SHAN[1], Tao XIE[1]

([1]*State Key Laboratory of Robotics and System, Harbin Institute of Technology, Harbin 150001, China*)

([2]*College of Computer and Control Engineering, Qiqihar University, Qiqihar 161006, China*)

†E-mail: wanghongyan1993@163.com

Received Dec. 17, 2011; Revision accepted May 7, 2012; Crosschecked May 29, 2012

Abstract: This paper presents a type of vibration energy harvester combining a piezoelectric cantilever and a single degree of freedom (SDOF) elastic system. The main function of the additional SDOF elastic system is to magnify vibration displacement of the piezoelectric cantilever to improve the power output. A mathematical model of the energy harvester is developed based on Hamilton's principle and Rayleigh-Ritz method. Furthermore, the effects of the structural parameters of the SDOF elastic system on the electromechanical outputs of the energy harvester are analyzed numerically. The accuracy of the output performance in the numerical solution is identified from the finite element method (FEM). A good agreement is found between the numerical results and FEM results. The results show that the power output can be increased and the frequency bandwidth can be improved when the SDOF elastic system has a larger lumped mass and a smaller damping ratio. The numerical results also indicate that a matching load resistance under the short circuit resonance condition can obtain a higher current output, and so is more suitable for application to the piezoelectric energy harvester.

Key words: Piezoelectric cantilever, Single degree of freedom elastic (SDOF) system, Energy harvesting, Finite element analysis (FEA)

doi:10.1631/jzus.A1100344 **Document code:** A **CLC number:** TM619; TN384

1 Introduction

In recent years, a variety of wireless sensing applications or portable electronics have emerged. However, the batteries used to power these devices have some disadvantages, such as large volume, limited lifespan and high cost (Paradiso and Starner, 2005; Hudak and Amatucci, 2008; Mathuna *et al.*, 2008). Energy harvesting from a variety of ambient sources (heat, solar, wind, and vibration) provides potential solutions (Mateu and Moll, 2005; Beeby *et al.*, 2006; Ujihara *et al.*, 2007; Yuan *et al.*, 2009; Pei *et al.*, 2011). As one ubiquitous energy form in our daily life, vibration energy harvesting has attracted immense attention owing to its relatively low cost and high power density. Among the transduction mechanisms for converting the vibration energy into useful electrical energy (i.e., piezoelectric, electromagnetic, and electrostatic energy), the piezoelectric energy harvester is the simplest to fabricate. Therefore, it is well suited to small scale systems (Beeby *et al.*, 2006).

A conventional piezoelectric energy harvester is a cantilevered unimorph/bimorph structure with or without a tip mass. Such single degree of freedom (SDOF) cantilever-type devices provide the maximum power output when operating at resonance, but this condition is difficult to guarantee when the excitation is not controllable or is intrinsically frequency-variant over a broad bandwidth. To overcome this disadvantage, two innovative approaches

* Project supported by the National Natural Science Foundation of China (No. 51077018), and the Science and Technology Planning Project of Qiqihar (No. GYGG2010-02-1), China

have been considered. The first is to tune the resonance frequency of a single energy harvester so that it matches the frequency of the ambient vibration at all times (Wu *et al.*, 2006; Challa *et al.*, 2008; Eichhorn *et al.*, 2009). The second approach is to widen the bandwidth using multimodal energy harvesting method, coupled elastic structures or non-linear oscillation techniques (Xue *et al.*, 2008; Erturk *et al.*, 2009; Lee *et al.*, 2009; Tadesse *et al.*, 2009; Yang and Yang, 2009; Stanton *et al.*, 2010; Xu *et al.*, 2010). Other approaches, including optimizing parameters of the energy harvester (du Toit *et al.*, 2005; Liao and Sodano, 2008) and impedance matching technology (Liang and Liao, 2010; Kong *et al.*, 2010), have also been proposed to improve the power output of the energy harvester.

A different concept, the dynamic vibration absorber (or dynamic magnifier), which works through the interaction of coupled elastic structures, has been considered by some investigators (Cornwell *et al.*, 2005; Ma *et al.*, 2010). In these studies, the developed mathematical models ignore the electromechanical coupling of the energy harvester.

In a recent study, Aldraihem and Baz (2011) established an electromechanical model of piezoelectric rods with a dynamic magnifier and studied the effect of the design parameters of the dynamic magnifier on the power output. Tang and Zuo (2011) investigated the optimal power output of an energy harvester with a dynamic magnifier based on a two degree of freedom spring-mass model. Arafa *et al.* (2011) carried out experiments to demonstrate the feasibility of a cantilevered piezoelectric energy harvester with a dynamic magnifier. These researchers focused on the maximum power that can be achieved by ignoring damping of the dynamic magnifier. In reality, damping always exists and affects the performance of the energy harvester. Also, the two degree of freedom spring-mass model ignored many important parameters, such as the strain distribution in the energy harvesting structure, which plays a major role in determining energy harvester performance. Hence, it can provide only an analytical understanding of the energy harvesting problem.

The efficient design of an energy harvester requires an accurate model that can be used to evaluate quickly the effect of parameter variation on the device. Hamilton's principle and Rayleigh-Ritz method on modeling transverse vibration are popular. Hagood *et al*. (1990) provided a good starting point to model a cantilevered piezoelectric actuator/sensor. As applied by Sodano *et al*. (2004) and du Toit *et al*. (2005), a coupled electromechanical model for a cantilevered piezoelectric energy harvester was constructed. This model was used to study optimal energy harvesting problems, including the effect of load resistance and electromechanical coupling on power optimality (du Toit and Wardle, 2007; Liao and Sodano, 2008), beam shape optimization for power harvesting (Dietl and Garcia 2010), and the tip (proof) mass effect on vibration energy harvesting performance (du Toit *et al.*, 2005; Kim *et al.*, 2010).

Unlike previous studies on the effect of the beam shape or the tip (proof) mass geometry on power outputs of the piezoelectric cantilever, this paper focuses on the effect of the mass and the damping of the additional SDOF elastic system on the power outputs of a piezoelectric cantilever. A mathematical model for the energy harvester, combining a piezoelectric cantilever and a SDOF elastic system, is developed using Hamilton's principle and Rayleigh-Ritz method. The displacement and power amplifying abilities of the combined energy harvester are studied based on this model. The electrical outputs generated in matching load resistances under short circuit and open circuit resonance conditions are discussed. Finally, the validity of the developed mathematical model is verified using the finite element method (FEM).

2 Theoretical modeling

Fig. 1 shows the structure of the energy harvester combining a piezoelectric cantilever and a SDOF elastic system. The piezoelectric cantilever consists of two piezoelectric plates and a metallic plate. Two piezoelectric plates (PZT_1 and PZT_2) are bonded to the top and bottom of the metallic plate, respectively. The piezoelectric bimorphs are oppositely polarized in the z direction and are connected in series. The output terminal is directly connected to a resistor (R_L). One end of the metallic plate is connected to a SDOF elastic system consisting of a moving mass (M) connected to the base with a spring (K_1) and a parasitic damping element (C_1). The other end of the metallic beam is free.

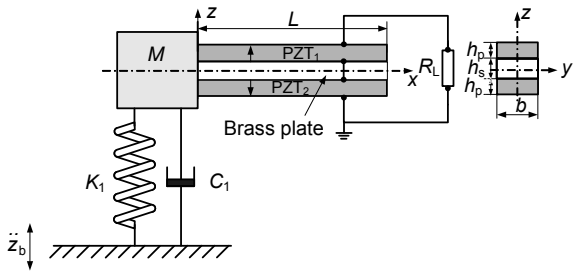

Fig. 1 Model of energy harvester combining a piezoelectric cantilever and a SDOF elastic system

L is the length of the piezoelectric beam, and h_p and h_s is the thickness of the piezoelectric plate and the metallic plate, respectively

For modeling, the assumption should be made that the PZT patches are perfectly bonded to the metallic plate and show linear elastic behavior. Another assumption is that the moving mass of the SDOF elastic system is considered as a lumped mass. The constitutive relations for the metallic material and the piezoelectric material can be written as (Auld, 1973)

$$T_s = c_s S_s \tag{1}$$

$$T_p = c_{11}^E S_p - e_{31} E, \tag{2}$$

$$D = e_{31} S_p + \varepsilon_{33}^S E, \tag{3}$$

where T is the stress, S is the strain. The subscripts s and p stand for the metallic material and the piezoelectric material, respectively. E is the electric field, D is the electrical displacement, c_s is the stiffness of the metallic beam, c_{11}^E is the stiffness of the piezoelectric material at constant electric field, e_{31} is the piezoelectric constant, and ε_{33}^S is the dielectric constant of the piezoelectric material at constant strain.

The dynamic equations of the energy harvesting system are derived using Hamilton's principle (Hagood *et al.*, 1990).

$$\int_{t_1}^{t_2} \left[\delta(T - U + W_e) + \delta W\right] \mathrm{d}t = 0, \tag{4}$$

where δ is the variation, t is time, T is the kinetic energy, U is the internal potential energy, W_e is the electric potential energy in the electrical field of the piezoelectric device, and W is the external work applied to the system. The sum of $T-U+W_e$ is called the Lagrangian L_a.

In an elastic body, the energies at all points within the structure are considered; hence, the piezoelectric beam will take the form of volume integrals. We assume that the motion of the piezoelectric beam is constrained to the transverse direction (z direction) and that the displacement w is non-zero. Let $w=z_m-z_M$, where z_m is the displacement of the piezoelectric beam, and z_M is the displacement of the SDOF elastic system, both relative to the base.

The individual energy terms and external work in Eq. (4) are defined as

$$T = \frac{1}{2} M \dot{z}_M^2 + \frac{1}{2} m \dot{z}_m^2 = \frac{1}{2} M \dot{z}_M^2 + \frac{1}{2} m \left(\dot{w} + \dot{z}_M\right)^2, \tag{5}$$

$$U = \frac{1}{2} K_1 z_M^2 + \frac{1}{2} \int_{V_p} S_p T_p \mathrm{d}V_p + \frac{1}{2} \int_{V_s} S_s T_s \mathrm{d}V_s, \tag{6}$$

$$W_e = \frac{1}{2} \int_{V_p} E D \mathrm{d}V_p, \tag{7}$$

$$\begin{aligned} \delta W = {} & (\delta z_M)(B_1 \ddot{z}_b) + \int_{V_p} (\delta w)(m \ddot{z}_b) \mathrm{d}V_p \\ & + \int_{V_s} (\delta w)(m \ddot{z}_b) \mathrm{d}V_s + \sum_{j=1}^{nq} \delta \varphi_j q_j, \end{aligned} \tag{8}$$

where M and m are the lumped masses of the SDOF elastic system and the piezoelectric beam, respectively, K_1 represents the stiffness of the SDOF elastic system, and $\dot{z}_M$ and $\dot{z}_m$ represent the velocities of the lumped masses of the SDOF elastic system and the piezoelectric beam, respectively. $\dot{w}$ is the velocity of the piezoelectric beam relative to the lumped mass of the SDOF system, V is the volume, B_1 represents the mass of the SDOF elastic system, $\ddot{z}_b$ is the input acceleration, and φ_j and q_j are the electrical potential and electrical charge for each of the nq electrode pairs, respectively.

The length of the piezoelectric beam L is much larger than the thickness h_s+2h_p and the width b. The piezoelectric beam is assumed to be an Euler-Bernoulli beam. Using the Raleigh-Ritz method, the vibration displacement of the piezoelectric beam can be written as

$$w = w(x,t) = \sum_{i=1}^{nr} \psi_{ri}(x) r_i(t) = \boldsymbol{\psi}_r(x) \boldsymbol{r}(t), \tag{9}$$

where $\boldsymbol{\psi}_r(x)$ is the assumed mode shape function vector, $\boldsymbol{r}(t)$ is the time-dependent generalized

mechanical coordinate, and *nr* is the number of modes. The bending mode shape of a clamped-free beam for the *i*th mode is given by

$$\psi_{ri}(x)=c\Bigg[(\cosh(\alpha_i x)-\cos(\alpha_i x))-\frac{\cosh(\alpha_i L)+\cos(\alpha_i L)}{\sinh(\alpha_i L)+\sin(\alpha_i L)}(\sinh(\alpha_i x)-\sin(\alpha_i x))\Bigg], \tag{10}$$

where c is an arbitrary constant. For the first bending mode of the piezoelectric cantilever, α_i=1.875/L.

The axial strain $S(x, t)$ is expressed in terms of the deflection $w(x, t)$ as

$$S(x,t)=-z\frac{\partial^2 w(x,t)}{\partial x^2}=-z\boldsymbol{\psi}_r''(x)\boldsymbol{r}(t), \tag{11}$$

where z is the position from the neutral axis.

This electrical potential term, $\varphi_j=\varphi(x_j, t)$, can be expressed via a potential distribution, $\phi_{vj}(x)$, and the generalized electrical voltage coordinate, $v_j(t)$, as follows:

$$\varphi(x,t)=\sum_{j=1}^{nq}\psi_{vj}(x)v_j(t)=\boldsymbol{\psi}_v(x)\boldsymbol{v}(t), \tag{12}$$

where $\boldsymbol{\psi}_v(x)$ is the electrical mode shape vector, and $\boldsymbol{v}(t)$ is the voltage over the load resistance.

The electric potential distribution can be given by

$$\psi_v=\begin{cases}\dfrac{(h_p+h_s/2)+z}{h_p}, & -\dfrac{h_s}{2}\le z\le -\dfrac{h_s}{2}-h_p,\\[2ex] \dfrac{-h_s/2+z}{h_p}, & \dfrac{h_s}{2}\le z\le \dfrac{h_s}{2}+h_p,\end{cases} \tag{13}$$

where h_p and h_s is the thickness of the piezoelectric plate and the metallic plate, respectively.

When the piezoelectric beam is connected to the load resistance R_L, the voltage $v(t)$ and the current $\dot{q}(t)$ are related by

$$v(t)=R_L\dot{q}(t). \tag{14}$$

Lagrange's equation for the system is given by

$$\begin{aligned}&\frac{\mathrm{d}}{\mathrm{d}t}\frac{\partial L_a}{\partial \dot{z}_M}-\frac{\partial L_a}{\partial z_M}=-B_1\ddot{z}_b,\\ &\frac{\mathrm{d}}{\mathrm{d}t}\frac{\partial L_a}{\partial \dot{r}}-\frac{\partial L_a}{\partial r}=-B_2\ddot{z}_b,\\ &\frac{\mathrm{d}}{\mathrm{d}t}\frac{\partial L_a}{\partial \dot{q}}-\frac{\partial L_a}{\partial q}=-R_L\dot{q}.\end{aligned} \tag{15}$$

where B_2 is the mass function of the piezoelectric beam, $B_2=m\boldsymbol{\psi}_r$.

From Eq. (15), the electromechanical equation of an energy harvester combining a piezoelectric bimorph cantilever and a SDOF elastic system can be obtained:

$$\begin{aligned}&(M+m)\ddot{z}_M+C_1\dot{z}_M+K_1z_M+B_2\ddot{r}=-B_1\ddot{z}_b,\\ &M_0\ddot{r}+C_2\dot{r}+K_0r-\theta v+B_2\ddot{z}_M=-B_2\ddot{z}_b,\\ &\theta\dot{r}+C_p\dot{v}+\frac{1}{R_L}v=0,\end{aligned} \tag{16}$$

where C_1 and C_2 is the mechanical damping of the SDOF elastic system and the piezoelectric beam, respectively.

In order to obtain a closed-form scalar equation, a single mode is considered. The mode shape function vector $\boldsymbol{\psi}_r(x)$ can then be approximated by the specific mode shape function $\psi_{ri}(x)$. In Eq. (16), the mass expression of the piezoelectric beam, M_0 is given by

$$M_0=\int_{V_p}\rho_s\psi_{ri}^2\mathrm{d}V_s+2\int_{V_p}\rho_p\psi_{ri}^2\mathrm{d}V_p. \tag{17}$$

The static mass of the piezoelectric beam, m is given by

$$m=\int_{V_S}\rho_s\mathrm{d}V_s+2\int_{V_p}\rho_p\mathrm{d}V_p. \tag{18}$$

The stiffness expression of the piezoelectric beam, K_0 is given by

$$K_0=\int_{V_S}c_s(-z\psi_{ri}'')^2\mathrm{d}V_s+2\int_{V_p}c_{11}^E(-z\psi_{ri}'')^2\mathrm{d}V_p. \tag{19}$$

The electromechanical coupling expression, θ is given by

$$\theta = \int_{V_p} \left(-z\psi_{ri}''\right) e_{31} (-\nabla \psi_v) \mathrm{d}V_p. \tag{20}$$

The capacitance term, C_p is given by

$$C_p = \frac{1}{2} \int_{V_p} \left(-\nabla \psi_v\right) \varepsilon_{33}^S \left(-\nabla \psi_v\right) \mathrm{d}V_p. \tag{21}$$

The input mass terms, B_1 and B_2, are given by

$$\begin{aligned} &B_1 = M, \\ &B_2 = m\psi_{ri} = \int_{V_S} \rho_s \psi_{ri} \mathrm{d}V_s + 2\int_{V_p} \rho_p \psi_{ri} \mathrm{d}V_p. \end{aligned} \tag{22}$$

From Eq. (16), the closed-form solution of the amplitude for the mechanical coordinate, output voltage and power can be obtained as follows:

$$\left|\frac{r}{\ddot{z}_b}\right| = \frac{1}{K_0} \frac{\sqrt{1+(\alpha\Omega_2)^2}\, B_2 \sqrt{(ug^2\Omega_2^2 - 1)^2 + (2\xi_1 g\Omega_2)^2}}{\sqrt{A^2 + B^2}}, \tag{23}$$

$$\left|\frac{V}{\ddot{z}_b}\right| = \frac{1}{|\theta|} \frac{\alpha k^2 \Omega_2 B_2 \sqrt{(ug^2\Omega_2^2 - 1)^2 + (2\xi_1 g\Omega_2)^2}}{\sqrt{A^2 + B^2}}, \tag{24}$$

$$\left|\frac{P}{\ddot{z}_b}\right| = \frac{\omega_2}{K_0} \frac{\alpha k^2 \Omega_2^2 B_2^2 \left[(ug^2\Omega_2^2 - 1)^2 + (2\xi_1 g\Omega_2)^2\right]}{A^2 + B^2}, \tag{25}$$

where

$$\begin{aligned} A^2 + B^2 = {} & \{(1-\Omega_2^2 - 2\xi_2\alpha\Omega_2^2)[(1+u)g^2\Omega_2^2 - 1] + u_1 u g^2 \Omega_2^4 \\ & + [(1+k^2-\Omega_2^2)\alpha\Omega_2 + 2\xi_2\Omega_2]2\xi_1 g\Omega_2\}^2 \\ & + \{[(1+k^2-\Omega_2^2)\alpha\Omega_2 + 2\xi_2\Omega_2][(1+u)g^2\Omega_2^2 - 1] \\ & + u_1 u\alpha g^2 \Omega_2^5 - [1-\Omega_2^2 - 2\xi_2\alpha\Omega_2^2]2\xi_1 g\Omega_2\}^2, \end{aligned} \tag{26}$$

where ω_1 and ω_2 is the natural frequency of the SDOF elastic system and the piezoelectric beam, respectively. g is the natural frequency ratio of the piezoelectric beam to the SDOF elastic system, Ω_2 is the frequency ratio of the piezoelectric beam, u is the mass ratio of the piezoelectric beam to the lumped mass of the SDOF elastic system, u_1 is the mass transfer coefficient of the piezoelectric cantilever, and ξ_1 and ξ_2 is the damping ratio of the SDOF elastic system and piezoelectric beam, respectively. k^2 is the effective electromechanical coupling coefficient and α is the time constant. These dimensionless parameters are defined as

$$\begin{aligned} &\omega_1 = \sqrt{\frac{K_1}{M}},\ \omega_2 = \sqrt{\frac{K_0}{M_0}},\ g = \frac{\omega_2}{\omega_1},\ \Omega_2 = \frac{\omega}{\omega_2},\ u = \frac{m}{M}, \\ &u_1 = \frac{B_2^2}{mM_0},\ \xi_1 = \frac{C_1}{2M\omega_1},\ \xi_2 = \frac{C_2}{2M_0\omega_2},\ k^2 = \frac{\theta^2}{K_0 C_p}, \\ &\alpha = \omega_2 R_L C_p. \end{aligned} \tag{27}$$

When $u\to\infty$ and $g\to 0$, Eqs. (23)–(25) can be reduced to:

$$\left|\frac{r}{\ddot{w}_b}\right| = \frac{1}{K_0} \frac{\sqrt{1+(\alpha\Omega_2)^2}\, B_2}{\sqrt{A^2 + B^2}}, \tag{28}$$

$$\left|\frac{V}{\ddot{z}_b}\right| = \frac{1}{|\theta|} \frac{\alpha k^2 \Omega_2 B_2}{\sqrt{A^2 + B^2}}, \tag{29}$$

$$\left|\frac{P}{\ddot{z}_b}\right| = \frac{\omega_2}{K_0} \frac{\alpha k^2 \Omega_2^2 B_2^2}{A^2 + B^2}, \tag{30}$$

where

$$\begin{aligned} A^2 + B^2 = {} & (1-\Omega_2^2 - 2\xi_2\alpha\Omega_2^2)^2 \\ & + [(1+k^2-\Omega_2^2)\alpha\Omega_2 + 2\xi_2\Omega_2]^2. \end{aligned} \tag{31}$$

Eqs. (28)–(30) are the electromechanical model of a single piezoelectric cantilever, and they confirm the results reported by du Toit *et al.* (2005) and Kim *et al.* (2010).

3 Numerical results

In this section, a numerical calculation is performed to compare the performance of an energy harvester combining a piezoelectric cantilever and a SDOF elastic system with that of a single piezoelectric cantilever. Table 1 lists the material and geometric parameters of the piezoelectric beam, where C_{11}^E, e_{31} and ε_{33}^S are calculated according to du Toit (2005). The piezoelectric beam stiffness at constant electric field, C_{11}^E, is given by $C_{11}^E = 1/S_{11}^E$. The piezoelectric constant relating stress field, e_{31}, is given by

$e_{31}=d_{31}/S_{11}^{E}$. The absolute permittivity at constant strain, ε_{33}^{S}, is given by $\varepsilon_{33}^{S}=\varepsilon_{33}^{T}-2d_{31}e_{31}$, where ε_{33}^{T} is the absolute permittivity at constant stress.

Table 1 Material and geometric properties of the piezoelectric beam

Item	Value
Piezoelectric plate, ρ_p (kg/m^3)	7500
Substrate plate density, ρ_s (kg/m^3)	8920
Piezoelectric plate compliance, S_{11}^{E} (m^2/N)	1.65×10^{-11}
Piezoelectric plate stiffness, C_{11}^{E} (GPa)	60.6
Substrate plate stiffness, C_s (GPa)	113
Strain constant, d_{31} (C/N)	-2.74×10^{-10}
Stress constant, e_{31} (C/m^2)	−16.6
Vacuum permittivity, ε_0 (F/m)	8.854×10^{-12}
Absolute permittivity, ε_{33}^{T} (F/m)	$3400\varepsilon_0$
Absolute permittivity, ε_{33}^{S} (F/m)	$2372\varepsilon_0$
Beam length, L (mm)	60
Beam width, b (mm)	20
Thickness of piezoelectric layer, h_p (mm)	0.2
Thickness of substrate layer, h_s (mm)	0.3
Damping ratio of SDOF elastic system, ξ_1	0.002
Damping ratio of piezoelectric beam, ξ_2	0.02

Figs. 2a and 2b show the relative motion (w_{tip}/z_b) of the piezoelectric cantilever and the relative motion (z_M/z_b) of the SDOF elastic system for the combined energy harvester with different mass ratios, u, when g=1 and R_L=9.8 kΩ, respectively. In Fig. 2a, the relative motion (w_{tip}/z_b) of the combined piezoelectric energy harvester with different mass ratios is compared with that of a single piezoelectric cantilever, where w_{tip} is the tip displacement of the piezoelectric cantilever and z_b is the base displacement. The combined energy harvester generates two peaks (Fig. 2a) which are very sensitive to the mass ratio. As the mass ratio, u, decreases, both the left and right peaks increase, and the distance between the two peaks narrows, forming a wide-band frequency window. In a special case, as the mass ratio u=0.105, there exists a minimum relative motion between the two peaks, which is equal to the maximum relative motion of the single piezoelectric cantilever. In addition, for a given mass of the piezoelectric beam m, as the mass ratio $u=1\times10^{10}$ ($u\to\infty$) and the natural frequency ratio $g=1\times10^{-10}$ ($g\to0$), the relative motion curve of the combined piezoelectric energy harvester is identical to that of the single piezoelectric cantilever (Fig. 2a). The reason is that according to the equations $\omega_1=\sqrt{K_1/M}$, $g=\omega_2/\omega_1$ and $u=m/M$ in Eq. (27), the equations of the lumped mass and the spring stiffness are obtained as $M=m/u$ and $K_1=\omega_2^2M/g^2$, respectively. As $u=1\times10^{10}$ ($u\to\infty$) and $g=1\times10^{-10}$ ($g\to0$) for a given m and ω_2, $M=6.8\times10^{-13}$ ($M\to0$) and $K_1=2.15\times10^{13}$ ($K_1\to\infty$). Essentially, as the lumped mass $M\to0$ and the spring stiffness $K_1\to\infty$, the SDOF elastic system invalidates and the combined piezoelectric energy harvester is reduced to a single piezoelectric cantilever.

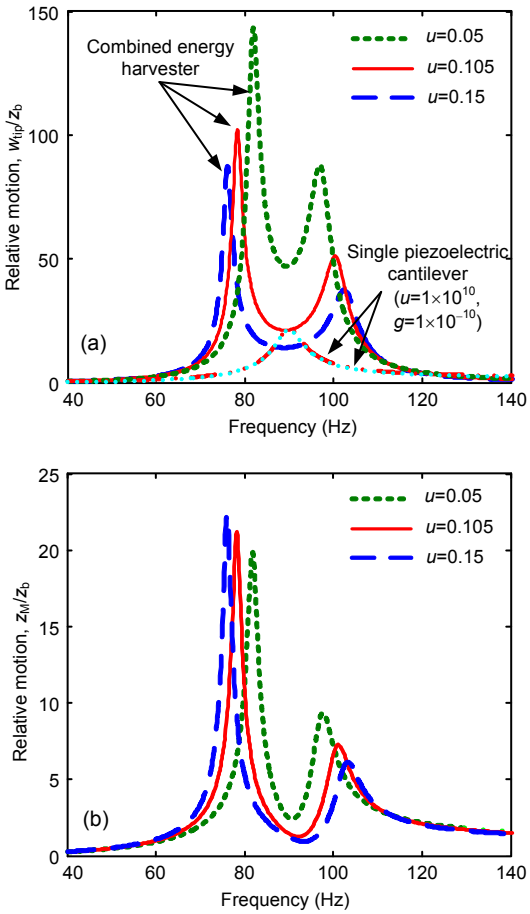

Fig. 2 Relative motion of the combined energy harvester with different mass ratios u when g=1 and R_L=9.8 kΩ
(a) Piezoelectric cantilever; (b) SDOF elastic system

In Fig. 2b, z_M is the displacement of the lumped mass M. The relative motion (z_M/z_b) of the SDOF elastic system is also very sensitive to the mass ratio. As the mass ratio, u, decreases, the left peak decreases

and the right peak increases. Compared with the relative motion (w_{tip}/z_b) of the piezoelectric cantilever (Fig. 2a), as the mass ratio, u, decreases, the left peak relative motion of the SDOF elastic system decreases, while the tip displacement of the piezoelectric beam increases. This shows that some mechanical energy is transferred to the piezoelectric beam from the SDOF elastic system at the left resonance frequency. However, as the mass ratio, u, decreases, both the right peak relative motion of the SDOF elastic system and the piezoelectric beam increase. This shows that the mechanical energy transferred to the SDOF elastic system from the piezoelectric beam is less than the increase in the mechanical energy of the piezoelectric beam because of the improvement resulting from the vibration displacement. The analytical results show that the additional spring-mass system can magnify the tip displacement of the piezoelectric beam when a proper mass ratio is used for the combined energy harvester.

Fig. 3 shows the output power of the energy harvester with different mass ratios, u, when g=1 and R_L=9.8 kΩ. A semi-logarithmic coordinate is used for displaying the difference of each power output curve more clearly. The output power (Fig. 3) behaves similar to the relative motion (w_{tip}/z_b) of the combined energy harvester (Fig. 2a). A smaller mass ratio u leads to a higher power output. In addition, as the mass ratio u=1×10^{10} ($u\to\infty$) and the natural frequency ratio g=1×10^{-10} ($g\to0$), the power graph of the combined piezoelectric energy harvester is identical to that of the single piezoelectric cantilever.

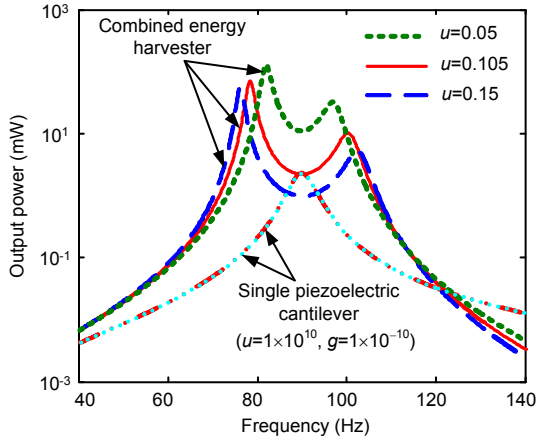

Fig. 3 Output power for a single and a combined energy harvester with different mass ratios u when g=1 and R_L=9.8 kΩ. Excitation acceleration is 9.8 m/s^2

Fig. 4 shows the effect of the damping ratio (ξ_1) of the additional SDOF elastic system on the output power when g=1, u=0.105 and R_L=9.8 kΩ. The increase in ξ_1 leads to a decrease in the peak power of the energy harvester. In particular, as the damping ratio of the SDOF elastic system ξ_1 is far larger than that of the piezoelectric cantilever, the dynamic magnified function of the additional SDOF elastic system becomes too weak to increase the peak power output of the piezoelectric cantilever. This shows that a proper damping ratio for the additional SDOF elastic system should be determined to improve the power output of the piezoelectric cantilever.

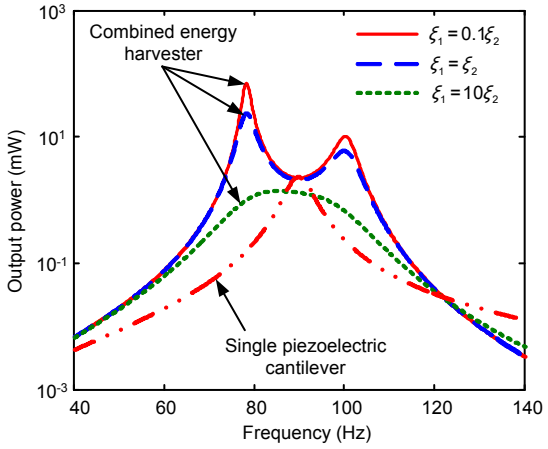

Fig. 4 Output power for a single and a combined energy harvester with different damping ratios ξ_1 when g=1, u=0.105 and R_L=9.8 kΩ. Excitation acceleration is 9.8 m/s^2

The maximum power output of a piezoelectric cantilever can be obtained at resonance frequency and anti-resonance frequency for short circuit condition ($R_L\to0$) and open circuit condition ($R_L\to\infty$), respectively (du Toit *et al.*, 2005; Kim *et al.*, 2010). According to the calculation equation of the natural frequencies $f=\sqrt{K_{eff}/M_0}/(2\pi)$, the resonance and anti-resonance frequencies can be determined from their respective effective stiffness, K_{eff}. The effective stiffness under short-circuit and open-circuit conditions are K_0 and $K_0(1+k^2)$, respectively. For the single piezoelectric cantilever, the resonance and anti-resonance frequencies are calculated as f_r=89.3 Hz and f_{ar}=94 Hz, respectively. Fig. 5 shows the variation in the output power of the single piezoelectric cantilever with load resistance at the resonance and anti-resonance frequencies. Both power graphs display peak values which correspond to the optimal load resistance. The two optimal load resistances are the

matching resistors of the piezoelectric element at the resonance and anti-resonance frequencies, $R_{opt,r}$= 9.8 kΩ and $R_{opt,ar}$=73.3 kΩ, respectively.

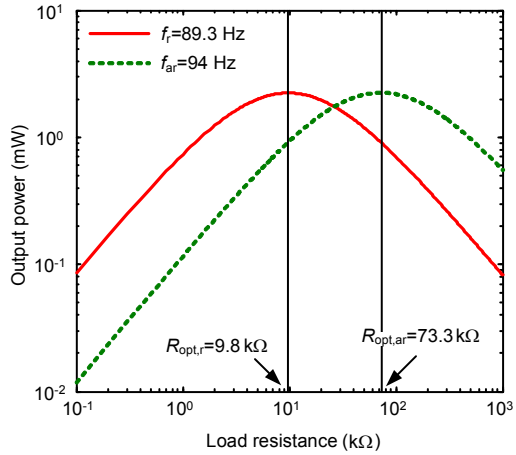

Fig. 5 Variation in output power of a single piezoelectric cantilever with load resistance at the resonance and anti-resonance frequencies. Excitation acceleration is 9.8 m/s^2

Figs. 6 and 7 illustrate the output voltage and output current of the energy harvester for two different load resistances when g=1 and u=0.105, respectively. A larger peak voltage is generated at a load resistance of 73.3 kΩ (Fig. 6). A larger peak current is generated at a load resistance of 9.8 kΩ (Fig. 7). Thus, a matching resistor ($R_{opt,ar}$=73.3 kΩ) at anti-resonance frequency is more suitable for applications requiring high voltage, and a matching resistor ($R_{opt,r}$=9.8 kΩ) at resonance frequency is more suitable for applications requiring high current. This conclusion is consistent with the comment on the high current and high voltage operation presented by Renno *et al.* (2009). Also, the connecting of different load resistances results in the movement of the bandwidth of the energy harvester along the frequency axis. The reason is that an increase in load resistance leads to an increase in the effective stiffness of the piezoelectric cantilever. Accordingly, the resonance frequency of the energy harvester also increases.

Fig. 8 shows the output power of the energy harvester for two optimal load resistances when g=1 and u=0.105. Note that the peak power generated at a load resistance of 73.3 kΩ is close to that generated at a load resistance of 9.8 kΩ. Thus, the use of matching load resistances under the resonance and anti-resonance frequency conditions produces almost the same amount of maximum power although they have different voltage and current outputs.

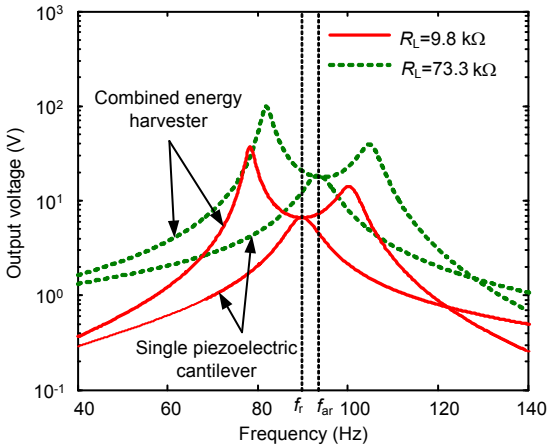

Fig. 6 Output voltage vs. vibration frequency for two different load resistances when g=1 and u=0.105. Excitation acceleration is 9.8 m/s^2

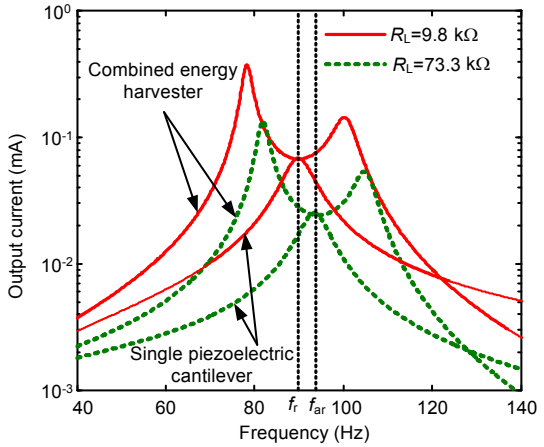

Fig. 7 Output current vs. vibration frequency for two different load resistances when g=1 and u=0.105. Excitation acceleration is 9.8 m/s^2

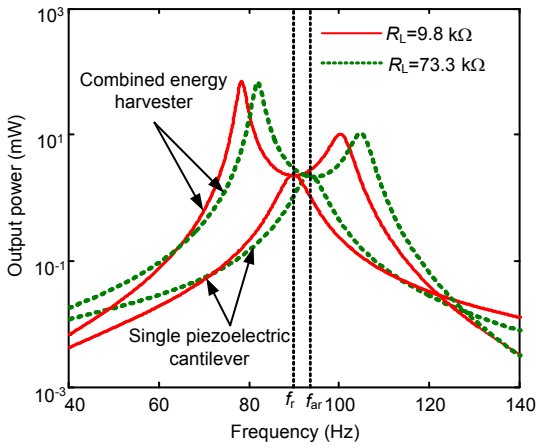

Fig. 8 Output power vs. vibration frequency for two different load resistances when g=1 and u=0.105. Excitation acceleration is 9.8 m/s^2

4 Finite element verification

In this section, an FE model is developed in ANSYS® software to analyze the performance of the energy harvester and validate the numerical results obtained from the analytical model mentioned above.

Fig. 9 shows the FE model of the combined energy harvester. In this model, the piezoelectric cantilever beam has a sandwich structure, in which two piezoelectric layers are bonded to the top and bottom of the central brass beam. Note that the adhesive layers between the metallic beam and piezoelectric layers are ignored because of negligible thickness. The 8-node hexahedral coupled-field element SOLID5 is used for the PZT layers. The 8-node linear structural element SOLID45 is used for the brass beam. The point element MASS21 is used for the lumped mass (M) of the SDOF system. The spring-damping element COMBIN14 is used for the spring (K_1) of the SDOF elastic system. The piezoelectric circuit element CIRCU94 is used to model the load resistance for generating voltage, current and power outputs.

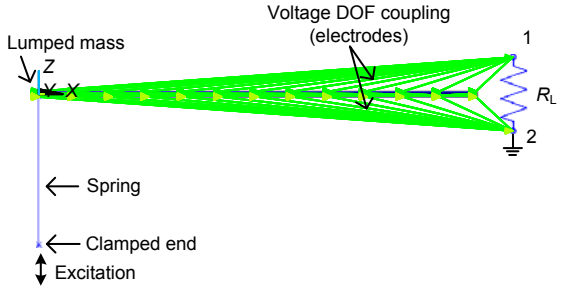

Fig. 9 Finite element model of the energy harvester combining a piezoelectric cantilever and a SDOF elastic system

The polarization direction of the piezoelectric material is represented by the sign of the piezoelectric constants d_{31}, d_{33} and d_{15}. 3D parameters of PZT-5H used in FEA are given by Wang (1983). When the top and bottom piezoelectric layers are connected in series, they are configured in an opposite polarization direction. Hence, d_{31}, d_{33} and d_{15} for the bottom piezoelectric layer have a sign in defined material property opposite to those of the top piezoelectric layer. The voltage degrees at FE nodes on the two electrode surfaces facing the central brass layer are connected by using the "couple" command for implementing a uniform electrical potential. Similarly, the voltage degrees at FE nodes on the upper electrode surface are coupled to common node "1" and those on the bottom electrode surface are coupled to common node "2". These two common nodes are used to connect with the external load resistance. Note that both the bottom electrode surface and node "2" are grounded.

In this FE model, the Rayleigh damping is considered for the combined energy harvesting structure, which is given by

$$\boldsymbol{C}=\alpha\boldsymbol{M}+\beta\boldsymbol{K}, \tag{32}$$

where α and β are constants. The damping matrix, $\boldsymbol{C}$, is given by

$$\boldsymbol{C}=\begin{bmatrix} C_1+C_2 & -C_2 \\ -C_2 & C_2 \end{bmatrix}. \tag{33}$$

The mass matrix, $\boldsymbol{M}$, is given by

$$\boldsymbol{M}=\begin{bmatrix} M & 0 \\ 0 & M_0 \end{bmatrix}. \tag{34}$$

The stiffness matrix, $\boldsymbol{K}$, is given by

$$\boldsymbol{K}=\begin{bmatrix} K_1+K_0 & -K_0 \\ -K_0 & K_0 \end{bmatrix}. \tag{35}$$

The application of the modal matrix, $\boldsymbol{P}$, results in

$$\begin{aligned}\boldsymbol{P}^{\mathrm{T}}\boldsymbol{C}\boldsymbol{P}&=\alpha\boldsymbol{P}^{\mathrm{T}}\boldsymbol{M}\boldsymbol{P}+\beta\boldsymbol{P}^{\mathrm{T}}\boldsymbol{K}\boldsymbol{P}\\&=\begin{bmatrix} \alpha+\beta\omega_1^2 & \\ & \alpha+\beta\omega_2^2 \end{bmatrix}.\end{aligned} \tag{36}$$

Using Eq. (36), two parameters of the Rayleigh damping, α and β, can be determined. Note that when the mass or the structural stiffness of the energy harvester is changed, the Rayleigh damping also changes.

Tables 2 and 3 list the resonance frequency and the output power of analytical results and FEA results with two different load resistances of 9.8 kΩ and 73.3 kΩ, respectively. The FEA results are in good agreement with the analytical results. The validity of the mathematical model with respect to the electromechanical output is identified by the FEM.

Table 2 Comparison between the analytical and FEA results with a mass ratio of 0.105 and a load resistance of 9.8 kΩ when g=1. Excitation acceleration is 9.8 m/s^2

Node	Analytical results		FEA results	
	Frequency (Hz)	Power (mW)	Frequency (Hz)	Power (mW)
Left peak	78.3	67.7	80	63.8
Middle well	89.3	1.95	92	2.83
Right peak	100.3	9.7	102.5	13.3

Table 3 Comparison between the analytical and FEA results with a mass ratio of 0.105 and a load resistance of 73.3 kΩ when g=1. Excitation acceleration is 9.8 m/s^2

Node	Analytical results		FEA results	
	Frequency (Hz)	Power (mW)	Frequency (Hz)	Power (mW)
Left peak	82.2	66.4	83.5	63.1
Middle well	94	2.21	95.5	2.05
Right peak	104.5	11.0	106.5	13.2

Fig. 10 shows the output power obtained from FEA with different mass ratios when R_L=9.8 kΩ. The smaller mass ratio u leads to a higher output power and a closer peak distance. As u=1×10^{10} and g=1×10^{-10} for a given m and ω_2, the relative motion curve of the combined piezoelectric energy harvester is nearly identical to that of the single piezoelectric cantilever. The FEA results are in good agreement with the numerical results. The validity of the analytical model is validated by the FEA method.

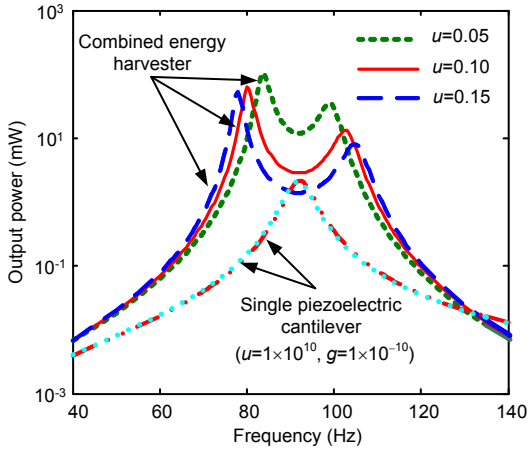

Fig. 10 Output power from system-level FEA with different mass ratios when g=1 and R_L=9.8 kΩ. Excitation acceleration is 9.8 m/s^2

Fig. 11 shows the output power obtained from FEA with different damping ratios ξ_1 when R_L=9.8 kΩ and u=0.105. An increase in ξ_1 leads to a decrease in the peak power of the energy harvester. A good agreement is also found between the FEA and numerical results.

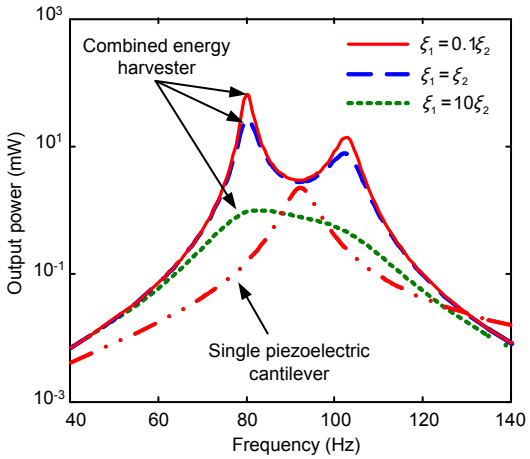

Fig. 11 Output power from system-level FEA with different damping ratios when g=1, R_L=9.8 kΩ and u=0.105. Excitation acceleration is 9.8 m/s^2

5 Conclusions

Based on Hamilton's principle and the Rayleigh-Ritz method, a mathematical model of an energy harvester combining a piezoelectric cantilever and a SDOF elastic system was developed. The results obtained from the mathematical model were in very good agreement with those from FEM. Some conclusions can be drawn as follows.

1. The additional SDOF elastic system can increase the power output of the piezoelectric cantilever and improve the frequency bandwidth when the mass ratio of the piezoelectric cantilever to the lumped mass of SDOF elastic system is below 0.105.

2. A larger damping ratio seriously weakens the function of the SDOF elastic system as a displacement magnifier and decreases the power output. Hence, a proper damping ratio for the additional SDOF elastic system should be determined to improve the power output of the piezoelectric cantilever.

3. Two matching load resistances under short circuit and open circuit resonance conditions can obtain the same amount of maximal power. However, a matching load resistance under short circuit

resonance condition can obtain higher current output, and hence is more suitable for applications requiring a high current, such as a piezoelectric energy harvester.

References

Aldraihem, O., Baz, A., 2011. Energy harvester with dynamic magnifier. *Journal of Intelligent Material Systems and Structures*, **22**(6):521-530. [doi:10.1177/1045389X11402706]

Arafa, M., Akl, W., Aladwani, A., Aldraihem, O., Baz, A., 2011. Experimental Implementation of a Cantilevered Piezoelectric Energy Harvester with a Dynamic Magnifier. Proceedings of SPIE, the International Society for Optical Engineering, **7977**:79770Q. [doi:10.1117/12.880689]

Auld, B.A., 1973. Acoustic Fields and Waves in Solids. Wiley, New York, p.357-382.

Beeby, S.P., Tudor, M.J., White, N.M., 2006. Energy harvesting vibration sources for microsystems applications. *Measurement Science and Technology*, **17**(12):R175-R195. [doi:10.1088/0957-0233/17/12/R01]

Challa, V.R., Prasad, M.G., Shi, Y., Fisher, F.T., 2008. A vibration energy harvesting device with bidirectional resonance frequency tunability. *Smart Materials and Structures*, **17**(1):015035. [doi:10.1088/0964-1726/17/01/015035]

Cornwell, P.J., Goethal, J., Kowko, J., Damianakis, M., 2005. Enhancing power harvesting using a tuned auxiliary structure. *Journal of Intelligent Material Systems and Structures*, **16**(10):825-834. [doi:10.1177/1045389X05055279]

Dietl, J.M., Garcia, E., 2010. Beam shape optimization for power harvesting. *Journal of Intelligent Material Systems and Structures*, **21**(6):633-646. [doi:10.1177/1045389X10365094]

du Toit, N., 2005. Modeling and Design of a MEMS Piezoelectric Vibration Energy Harvester. MS Thesis, Massachusetts Institute of Technology, USA.

du Toit, N., Wardle, B.L., 2007. Experimental verification of models for microfabricated piezoelectric vibration energy harvesters. *AIAA Journal*, **45**(5):1126-1137. [doi:10.2514/1.25047]

du Toit, N., Wardle, B.L., Kim, S.G., 2005. Design considerations for MEMS-scale piezoelectric mechanical vibration energy harvesters. *Integrated Ferroelectrics*, **71**(1):121-160. [doi:10.1080/10584580590964574]

Eichhorn, C., Goldschmidtboeing, F., Woias, P., 2009. Bidirectional frequency tuning of a piezoelectric energy converter based on a cantilever beam. *Journal of Micromechanics and Microengineering*, **19**(9):094006. [doi:10.1088/0960-1317/19/9/094006]

Erturk, A., Renno, J.M., Inman, D.J., 2009. Modeling of piezoelectric energy harvesting from an L-shaped beam-mass structure with an application to UAVs. *Journal of Intelligent Material Systems and Structures*, **20**(5):529-544. [doi:10.1177/1045389X08098096]

Hagood, N.W., Chung, W., Von Flotow, A., 1990. Modelling of piezoelectric actuator dynamics for active structural control. *Journal of Intelligent Material Systems and Structures*, **1**(3):327-354. [doi:10.1177/1045389X9000100305]

Hudak, N.S., Amatucci, G.G., 2008. Small-scale energy harvesting through thermoelectric, vibration, and radio frequency power conversion. *Journal of Applied Physics*, **103**(10):101301. [doi:10.1063/1.2918987]

Kim, M., Hoegen, M., Dugundji, J., Wardle, B., 2010. Modeling and experimental verification of proof mass effects on vibration energy harvester performance. *Smart Materials and Structures*, **19**(4):045023. [doi:10.1088/0964-1726/19/4/045023]

Kong, N.A., Ha, D.S., Etrurk, A., Inman, D.J., 2010. Resistive impedance matching circuit for piezoelectric energy harvesting. *Journal of Intelligent Material Systems and Structures*, **21**(13):1293-1302. [doi:10.1177/1045389X09357971]

Lee, S., Youn, B.D., Jung, B.C., 2009. Robust segment-type energy harvester and its application to a wireless sensor. *Smart Materials and Structures*, **18**(9):095021. [doi:10.1088/0964-1726/18/9/095021]

Liang, J., Liao, W.H., 2010. Impedance Matching for Improving Piezoelectric Energy Harvesting Systems. Proceedings of SPIE, the International Society for Optical Engineering, **7643**:76430K. [doi:10.1117/12.847524]

Liao, Y.B., Sodano, H.A., 2008. Model of a single mode energy harvester and properties for optimal power generation. *Smart Materials and Structures*, **17**(6):065026. [doi:10.1088/0964-1726/17/6/065026]

Ma, P.S., Kim, J.E., Kim, Y.Y., 2010. Power-Amplifying Strategy in Vibration-Powered Energy Harvesters. Proceedings of SPIE, the International Society for Optical Engineering, **7643**:76430O. [doi:10.1117/12.848903]

Mateu, L., Moll, F., 2005. Review of Energy Harvesting Techniques and Applications for Microelectronics. Proceedings of SPIE, the International Society for Optical Engineering, p.359-373. [doi:10.1117/12.613046]

Mathuna, C.O., O'Donnell, T., Martinez-Catala, R.V., Rohan, J., O'Flynn, B., 2008. Energy scavenging for long-term deployable wireless sensor networks. *Talanta*, **75**(3):613-623. [doi:10.1016/j.talanta.2007.12.021]

Paradiso, J.A., Starner, T., 2005. Energy scavenging for mobile and wireless electronics. *IEEE Pervasive Computing*, **4**(1):18-27. [doi:10.1109/MPRV.2005.9]

Pei, G., Li, Y.Z., Li, J., Ji, J., 2011. Performance evaluation of a micro turbo-expander for application in low-temperature solar electricity generation. *Journal of Zhejiang University SCIENCE-A (Applied Physics and Engineering)*, **12**(3):207-213. [doi:10.1631/jzus.A1000105]

Renno, J.M., Daqaq, M.F., Inman, D.J., 2009. On the optimal energy harvesting from a vibration source. *Journal of Sound and Vibration*, **320**(1-2):386-405. [doi:10.1016/j.jsv.2008.07.029]

Sodano, H.A., Park, G., Inman, D.J., 2004. Estimation of electric charge output for piezoelectric energy harvesting.

Strain, **40**(2):49-58. [doi:10.1111/j.1475-1305.2004.00120.x]

Stanton, S.C., McGehee, C.C., Mann, B.P., 2010. Nonlinear dynamics for broadband energy harvesting: investigation of a bistable piezoelectric inertial generator. *Physica D: Nonlinear Phenomena*, **239**(10):640-653. [doi:10.1016/j.physd.2010.01.019]

Tadesse, Y., Zhang, S., Priya, S., 2009. Multimodal energy harvesting system: piezoelectric and electromagnetic. *Journal of Intelligent Material Systems and Structures*, **20**(5):625-632. [doi:10.1177/1045389X08099965]

Tang, X.D., Zuo, L., 2011. Enhanced vibration energy harvesting using dual-mass systems. *Journal of Sound and Vibration*, **330**(21):5199-5209. [doi:10.1016/j.jsv.2011.05.019]

Ujihara, M., Carman, G.P., Lee, G.G., 2007. Thermal energy harvesting device using ferromagnetic materials. *Applied Physics Letters*, **91**(9):093508. [doi:10.1063/1.2775096]

Wang, J.R., 1983. Underwater Acoustical Material Manual. Science Press, Beijing, China (in Chinese).

Wu, W., Chen, Y., Lee, B., He, J., Peng, Y., 2006. Tunable Resonant Frequency Power Harvesting Devices. Proceedings of SPIE, the International Society for Optical Engineering, **6169**:61690A. [doi:10.1117/12.658546]

Xu, J.W., Shao, W.W., Kong, F.R., Feng, Z.H., 2010. Right-angle piezoelectric cantilever with improved energy harvesting efficiency. *Applied Physics Letters*, **96**(15):152904. [doi:10.1063/1.3374880]

Xue, H., Hu, Y., Wang, Q., 2008. Broadband piezoelectric energy harvesting devices using multiple bimorphs with different operating frequencies. *IEEE Transactions on Ultrasonics, Ferroelectrics, and Frequency Control*, **55**(9):2104-2108. [doi:10.1109/TUFFC.903]

Yang, Z., Yang, J., 2009. Connected vibrating piezoelectric bimorph beams as a wide-band piezoelectric power harvester. *Journal of Intelligent Material Systems and Structures*, **20**(5):569-574. [doi:10.1177/1045389X08100042]

Yuan, J.B., Xie, T., Shan, X.B., Chen, W.S., 2009. Resonant frequencies of a piezoelectric drum transducer. *Journal of Zhejiang University SCIENCE-A*, **10**(9):1313-1319. [doi:10.1631/jzus.A0820804]